

# BACKSTEPPING CONTROL OF A SWITCHED RELUCTANCE MOTOR WITH INTER-TURN SHORT-CIRCUIT

Mostafa ABDELOUHAB , Abdelilah ATTAR , Rachid ABOUTNI ,  
Jamal BOUCHNAIF 

Laboratory of Electrical and Maintenance Engineering, High School of Technology of Oujda,  
Mohammed First University, Bd Mohammed VI, P.O.Box 524, 60000 Oujda, Morocco

abelouhab.mostafa@ump.ac.ma, attar.abdelilah@gmail.com, aboutni@hotmail.com, j.bouchnaif@ump.ac.ma

DOI: 10.15598/aeee.v20i3.4326

Article history: Received Aug 15, 2021; Revised Jul 09, 2022; Accepted Jul 26, 2022; Published Sep 30, 2022.  
This is an open access article under the BY-CC license.

**Abstract.** *Improving the behavior of speed control in electric vehicles is currently a major challenge for researchers and engineers. For this study, we chose the context of a Switched Reluctance Motor (6/4 SRM) used in a hybrid Electric Vehicle with Extended Range (EREV). Speed regulation is an essential feature on long-distance trip. Speed regulators of backstepping type are very effective in this context given the non-linear nature of switched reluctance motors. The estimation of non-linear quantities, flux and inductance, uses Legendre polynomials. The control strategy uses four regulators, one for speed and three for stator currents. It is based on the Torque Sharing Function (TSF) and the Torque Inverse Model (TIM). Our simulation consists of studying the behavior of this type of control when an Inter-Turn Short-Circuit (ITSC) fault appears on one of the phases of the 6/4 SRM. In this paper, we are interested in temporal behavior of phasic currents and we will show the interest of these quantities as fault indicators allowing the real time diagnosis of this type of controller-machine.*

## Keywords

**Backstepping control, inter-turn short-circuit, switched reluctance motor.**

## 1. Introduction

Several non-linear modelling, non-linear control and diagnostic approaches have been developed in the past.

Nevertheless, we will limit ourselves to presenting those considered as the most interesting and up-to-date.

Several models can be used to equate the 6/4 SRM, for example, the flux model proposed by [1], which is the most appropriate for our study due to the need of equations allowing non-linear modelling for backstepping speed regulators [2], [3] and [4].

The estimation of the flux and inductance uses orthogonal Legendre polynomials. The evolution of these quantities as a function of the angular position  $\theta$  is done using a Fourier series decomposition [5].

The non-linear control strategy is based on Torque Sharing Function (TSF) [6] and Torque Inverse Model (TIM). The speed and current regulators are of the backstepping type [7] and [8] allowing rigorous control of these quantities with reduced torque ripple [9] and [10].

The separate model of the three phases of the 6/4 SRM motor will allow us to simulate short-circuit faults of the turns in one or more phases. The number of short-circuited turns has a linear influence on the resistance value and non-linear on the flux and inductance in the damaged phase [11].

Several fault indicators can be used such as (mean, standard deviation, maximum value and kurtosis) [12], we use RMS phasic currents as fault indicator to detect a short-circuit on a phase of the SRM.

This article aims to solve the problems with modelling, non-linear control, as well as diagnostics and fault tolerance of switched reluctance motors. Our objective is to show the possibilities offered by the backstepping control in terms of fault tolerance and

speed regulator monitoring of a 6/4 SRM 60 kW (circa 80 hp) around a setpoint speed of 300 rad·s<sup>-1</sup> (circa 3000 rpm).

## 2. Modelling Method

The main characteristics of the 6/4 SRM motor considered in our study are given in Tab. 1. The choice of this motor came from the fact that its model and its magnetization curve are available in MATLAB and Simulink, which will represent a reference model to validate our approach. This reference machine will be modeled without any additional mechanical load, the speed and position coder will be considered perfect to avoid the influence of any disturbances in our study. Indeed, only simulation makes it possible to isolate the study of a single disturbance among several.

**Tab. 1:** Summary of the parameters of the motor-rotor alone.

Useful power	60 kW
Nominal voltage	240 V
Resistance of a stator phase	0.05 Ω
Moment of inertia	0.0082 kg·m <sup>2</sup>
Viscous coefficient of friction	0.01 N·m·s
Maximum current per phase	450 A
Maximum flux	0.486 Wb

We consider a switched reluctance motor with an ITSC fault in the stator winding illustrated in Fig. 1, where  $\mu$  represent the short-circuit rate on phase 1 having  $n_s$  turns. Several models can be used to put into equation the 6/4 SRM, we propose to use the flux model. Equation (1) and Eq. (2) give the electrical and mechanical relations of this type of motor in the healthy case:

$$\begin{cases} V_1 = R_1 \cdot i_1 + \frac{d\varphi_1(\theta, i_1)}{dt}, \\ V_2 = R_2 \cdot i_2 + \frac{d\varphi_2(\theta, i_2)}{dt}, \\ V_3 = R_3 \cdot i_3 + \frac{d\varphi_3(\theta, i_3)}{dt}, \end{cases} \quad (1)$$

$$\begin{cases} w = \frac{d\theta}{dt}, \\ T_1 = \frac{1}{2} i_1^2 \frac{dL_1}{d\theta}, \\ T_2 = \frac{1}{2} i_2^2 \frac{dL_2}{d\theta}, \\ T_3 = \frac{1}{2} i_3^2 \frac{dL_3}{d\theta}, \\ T = T_1 + T_2 + T_3, \\ T - f \cdot w = J \cdot \frac{dw}{dt}, \end{cases} \quad (2)$$

where:

- $R_{123}$  and  $L_{123}$  represent resistors and inductances of the three phases,

- $V_{123}$ ,  $i_{123}$  and  $\varphi_{123}$  represent voltages, currents and flux of the three phases,
- $T_{123}$  and  $T$  represent torques of the three phases and total torque,
- $J$ ,  $f$ ,  $w$  and  $\theta$  represent moment of inertia, viscous coefficient of friction, instantaneous angular speed in rad·s<sup>-1</sup> and mechanical angular position in rad of motor-rotor alone.

To describe the non-linear behavior of 6/4 SRM, the estimation of the flux and inductance of the first phase according to the current which crosses it and of the angular position  $\theta$  is made using orthogonal Legendre polynomials. These polynomials are expressed as a function of the reduced variable  $x$  between  $-1$  and  $+1$ . To justify the order 13 of the chosen Legendre polynomial estimate, we provide a graphical plot in Fig. 2 to ensure that the function  $F_1$  is never equal to zero. This figure presents the case of the order 13 chosen, it is noted that this function presents the minimum risk of singularity with respect to the other orders between 3 and 15. The estimation of flux (Wb) is expressed by Eq. (3) and inductances (mH) is expressed by Eq. (4). The matrices  $\mathbf{A}$  and  $\mathbf{B}$  have a size (14, 4) and represent the numerical coefficients of the Legendre polynomials. This estimate is given without taking into account the angular position of the three phases, it is therefore necessary to introduce an angular shift according to the position of the stator teeth of the 6/4 SRM.

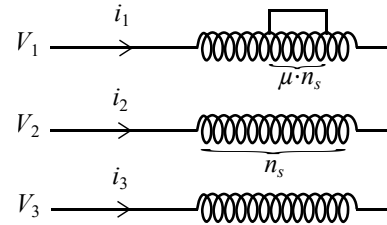


**Fig. 1:** Representation of the fault in the first phase.

$$\begin{bmatrix} \varphi_1(\theta, i_1) \\ \varphi_2(\theta, i_2) \\ \varphi_3(\theta, i_3) \end{bmatrix} = [\mathbf{A}(x)]^T \cdot \begin{bmatrix} 1 \\ \cos(4\theta) \\ \cos(8\theta) \\ \cos(12\theta) \end{bmatrix}, \quad (3)$$

$$\begin{bmatrix} L_1(\theta, i_1) \\ L_2(\theta, i_2) \\ L_3(\theta, i_3) \end{bmatrix} = [\mathbf{B}(x)]^T \cdot \begin{bmatrix} 1 \\ \cos(4\theta) \\ \cos(8\theta) \\ \cos(12\theta) \end{bmatrix}, \quad (4)$$

where  $\mathbf{A}(x) = [\mathbf{A}]^T \cdot [1 \ x \ x^2 \ x^3 \ \dots \ x^{13}]^T$ ,  $\mathbf{B}(x) = [\mathbf{B}]^T \cdot [1 \ x \ x^2 \ x^3 \ \dots \ x^{13}]^T$  and  $x = \frac{i_1 - 225}{225}$ .

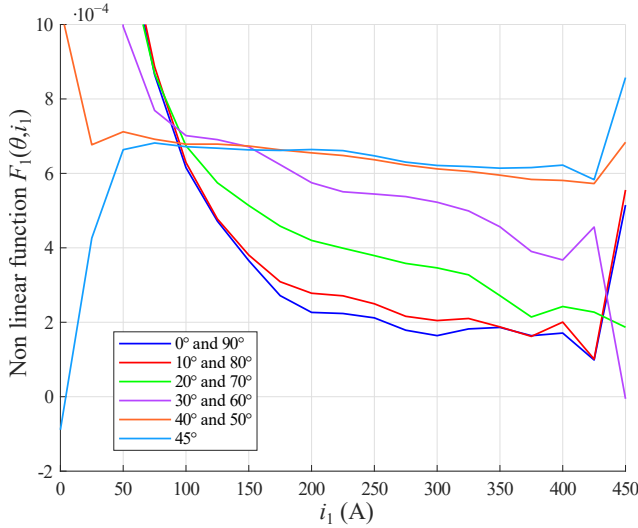


Fig. 2: Evolution of  $F_1 = \frac{\partial \phi_1}{\partial i_1}$  according to  $i_1$  and  $\theta$ .

### 3. Backstepping Controller Synthesis

The block diagram of the control method is presented in Fig. 3, where  $w^*$ ,  $T^*$  and  $i_{123}^*$  are the setpoint values of the different loops. Referring to the Eq. (1) and Eq. (2), we can represent our 6/4 SRM in Eq. (5) and Eq. (6) adapted to our strategy of command:

$$\begin{cases} V_1 = R_1 \cdot i_1 + \frac{\partial \varphi_1}{\partial i_1} \cdot \frac{di_1}{dt} + \frac{\partial \varphi_1}{\partial \theta} \cdot w, \\ V_2 = R_2 \cdot i_2 + \frac{\partial \varphi_2}{\partial i_2} \cdot \frac{di_2}{dt} + \frac{\partial \varphi_2}{\partial \theta} \cdot w, \\ V_3 = R_3 \cdot i_3 + \frac{\partial \varphi_3}{\partial i_3} \cdot \frac{di_3}{dt} + \frac{\partial \varphi_3}{\partial \theta} \cdot w, \\ \frac{1}{2} i_1^2 \frac{dL_1}{d\theta} + \frac{1}{2} i_2^2 \frac{dL_2}{d\theta} + \frac{1}{2} i_3^2 \frac{dL_3}{d\theta} - f \cdot w = J \cdot \frac{dw}{dt}, \\ w = \frac{d\theta}{dt}, \end{cases} \quad (5)$$

$$\begin{cases} \dot{x}_1 = \frac{\alpha_1 + u_1}{\beta_1}, \\ \dot{x}_2 = \frac{\alpha_2 + u_2}{\beta_2}, \\ \dot{x}_3 = \frac{\alpha_3 + u_3}{\beta_3}, \\ \dot{x}_4 = -\frac{f}{J} \cdot x_4 + \frac{1}{J} \cdot u_4, \end{cases} \quad (6)$$

where:

- $x_1 = i_1$ ,  $x_2 = i_2$ ,  $x_3 = i_3$  and  $x_4 = w$ ,
- $u_{123}$  represent control laws for the three current regulators.

$$T(i_1, i_2, i_3, \theta) = \frac{1}{2} i_1^2 \frac{dL_1}{d\theta} + \frac{1}{2} i_2^2 \frac{dL_2}{d\theta} + \frac{1}{2} i_3^2 \frac{dL_3}{d\theta}, \quad (7)$$

$$\begin{cases} \alpha_1 = -R_1 \cdot i_1 - \frac{\partial \varphi_1}{\partial \theta} \cdot w & \beta_1 = \frac{\partial \varphi_1}{\partial i_1}, \\ \alpha_2 = -R_2 \cdot i_2 - \frac{\partial \varphi_2}{\partial \theta} \cdot w & \beta_2 = \frac{\partial \varphi_2}{\partial i_2}, \\ \alpha_3 = -R_3 \cdot i_3 - \frac{\partial \varphi_3}{\partial \theta} \cdot w & \beta_3 = \frac{\partial \varphi_3}{\partial i_3}. \end{cases} \quad (8)$$

#### 1) Speed Regulator "Step 1"

Knowing that the error and the adjustment parameter of speed loop are denoted as  $z_4$  and  $C_w$ , the control law  $u_4$  for this regulator becomes as shown in Eq. (9):

$$u_4 = T^* = J \cdot \left( -C_w \cdot z_4 + \frac{f}{J} \cdot x_4 + \dot{w}^* \right). \quad (9)$$

#### 2) TSF and TIM Blocks

Before proceeding to the next step, we need the references of the three currents, the blocks TSF and TIM come to solve this problem and give the following transformation represented by Eq. (10):

$$T^* \xrightarrow{\text{TSF\&TIM}} (i_1^*, i_2^*, i_3^*). \quad (10)$$

The TSF strategy decomposes the total reference torque  $T^*$  into three setpoints  $T_1^*$ ,  $T_2^*$ , and  $T_3^*$  to be developed by each phase. Figure 4 illustrates the principle of this sinusoidal TSF, where  $\theta_{on}$ ,  $\theta_{off}$  and  $\theta_{ov}$  represent the angles of setting to 1, setting to 0 and overlap, respectively.

Three blocks TIM deduce the three setpoint currents  $i_1^*$ ,  $i_2^*$ ,  $i_3^*$  from the three setpoint torques generated by TSF block. Our original inversion of the torque is based on an approximate reversal, followed by a rigorous calculation as shown in Fig. 5. The approximate inversion is based on the quantified torque table. The rigorous calculation is based on determining the zero point of the difference between the non-linear function of the torque and the quantized value of the torque.

#### 3) Regulators of the Three Currents "Step 2"

Those regulators use  $i_{123}^*$  as virtual setpoints and  $u_{123}$  as real commands. Knowing that the current loop adjustment parameters are denoted  $C_1$ ,  $C_2$  and  $C_3$ , Eq. (11) gives the control laws  $u_1$ ,  $u_2$  and  $u_3$  for these regulators. The  $z_1$ ,  $z_2$  and  $z_3$  represent the three cur-

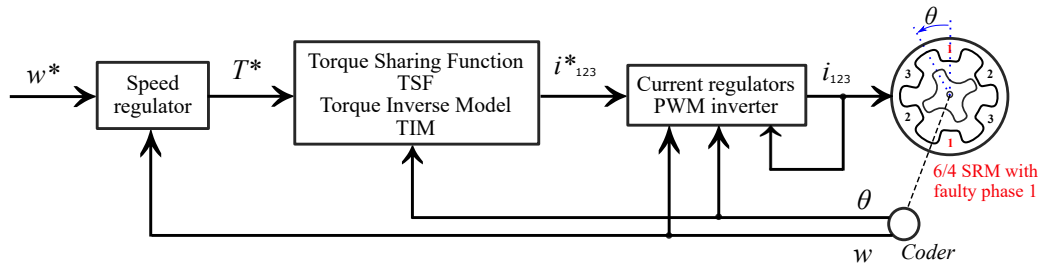


Fig. 3: Block diagram of the backstepping speed regulator.

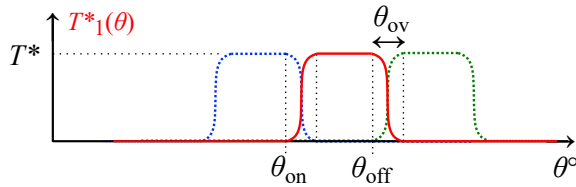


Fig. 4: Typical sinusoidal TSF profile.

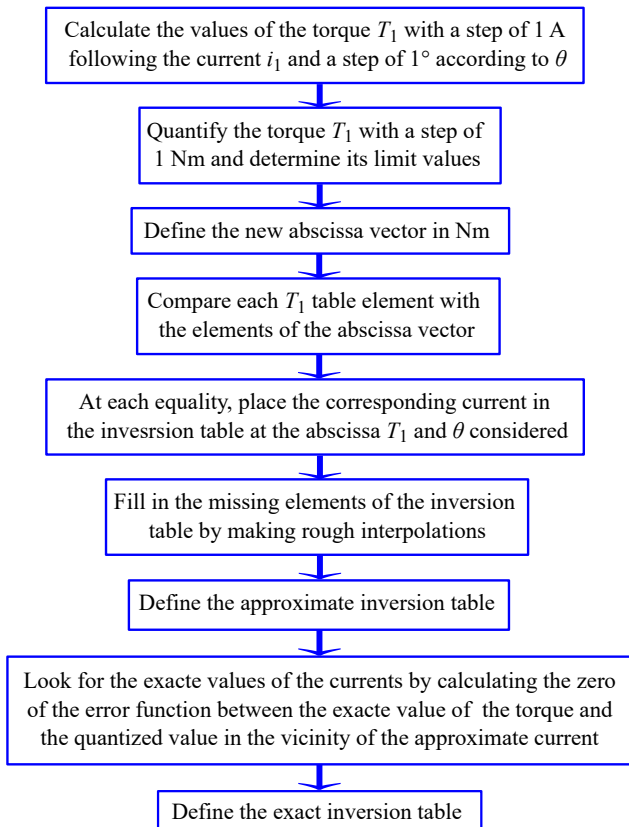


Fig. 5: Torque inversion algorithm for TIM.

rent regulator errors:

$$\begin{cases} u_1 = \left( -C_1 \cdot z_1 + \dot{i}_1^* \right) \cdot \beta_1 - \alpha_1, \\ u_2 = \left( -C_2 \cdot z_2 + \dot{i}_2^* \right) \cdot \beta_2 - \alpha_2, \\ u_3 = \left( -C_3 \cdot z_3 + \dot{i}_3^* \right) \cdot \beta_3 - \alpha_3. \end{cases} \quad (11)$$

#### 4) Definitions of Control Angles of Pulse Width Modulated Inverter

As can be seen in Fig. 6, a positive torque is developed in each phase only when it is supplied in its increasing inductance zone and when a total demagnetization zone of each phase is respected before starting a new cycle. Knowing that  $\theta_{on} \geq 45^\circ$ ,  $\theta_{off} \leq 90^\circ$  and  $\theta_{off} - \theta_{on} = 30^\circ$ , we can start our simulation with the following values:  $\theta_{on} = 45^\circ$  and  $\theta_{off} = 75^\circ$ . The modulation of the width of impulsion uses a triangular carrier of typical frequency of 10 kHz.

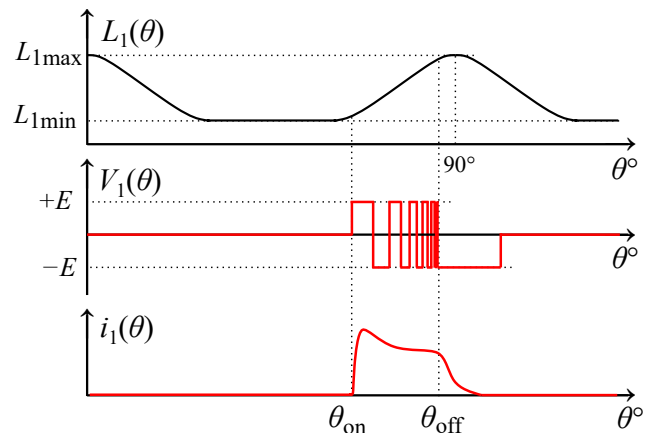


Fig. 6: Setting of the default control angles of the 6/4 SRM.

### 4. Open Loop Faultless Behavior

This part of simulation focuses on the open loop faultless behavior of the developed model. To validate our model, we compare it in an open loop with the reference model implemented in Matlab, the comparison context is as follows:

- To be able to compare the electrical and mechanical quantities of the two models, they must be supplied in an open loop with the same voltages. We are going to use the same converter blocks implemented in Matlab with a full wave command.

- The self-piloting of the two machines requires the installation of a command following  $\theta$  which will make it possible to successively switch the three arms of the power electronic converter to allow continuous rotation of those machines.

In terms of the validation of the nonlinear model developed, we can claim that it is very close to the block model included in Simulink Matlab. In fact, starting from the control voltages towards the angular speed and passing through the various electrical and mechanical quantities, it can be seen that the two models are comparable whether in transient mode or in permanent mode. The only differences are related to the voluntary limitation of the currents in order to avoid any divergence of the nonlinear functions involved. The following Tab. 2 shows the errors between the different average quantities of the reference model and the model developed over the entire simulation period (Mean error) and over the last 20 % of the simulation period representing the steady state (Relative error). The max-

**Tab. 2:** Summary table of validation of the developed model.

Temporal quantities	Mean error	Relative error
Voltages per phase	-1.1162 V	-0.5202 %
Flux per phase	-0.0012 Wb	-2.0996 %
Currents per phase	-0.0441 A	1.7962 %
Total torque	1.2783 Nm	6.1976 %
Angular speed	41.1346 rad·s <sup>-1</sup>	5.7625 %

imum steady-state error is at the torque level, but it remains around 6 % while the errors on the three electrical quantities do not exceed 2 %. We can therefore claim that the two models are similar from the point of view of errors and especially from the point of view of the shapes and forms of the different quantities.

## 5. Open Loop Fault Behavior

The following figures represent the open-loop temporal behavior of the phasic currents, phasic torques and angular speed of the 6/4 SRM. In our Simulink model, a limitation of the currents to 450 A was imposed to avoid any divergence of the Legendre polynomials. The results of this simulation are given for a short-circuit rate  $\mu$  which takes the values 5 %, 10 % and 15 % at times 0.5 s, 0.6 s and 0.7 s. Figure 7 shows that only the current in phase 1 increases with  $\mu$ . Figure 8 shows that the torque developed by the defective phase decreases with  $\mu$ . This figure also gives the shape of the total torque developed by this motor. Figure 9 gives the shape of the angular speed which decreases when the  $\mu$  increases. In the case of unsaturation [5], the phase inductances do not depend on the phase currents, so the electromagnetic torque produced by the SRM is reduced to Eq. (2). An additional fault torque

due to a high short circuit rate will certainly distort our study. In open loop, Fig. 7 and Fig. 8 show that the phase currents and torques have acceptable behaviors for a short-circuit rate not exceeding 15 %.

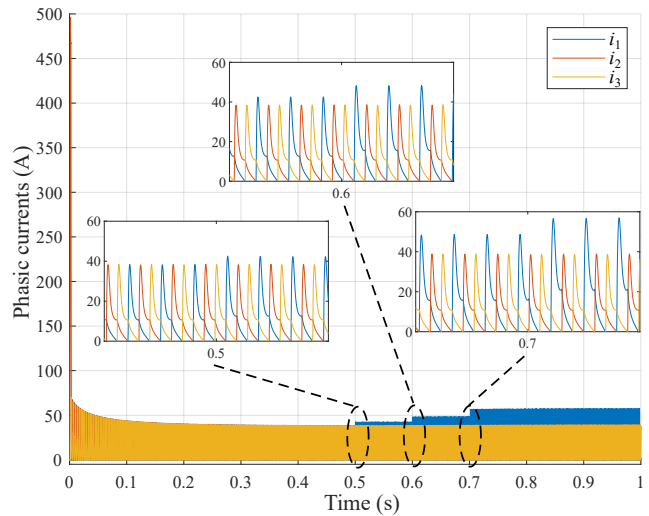


**Fig. 7:** Phasic currents in healthy and faulty cases.

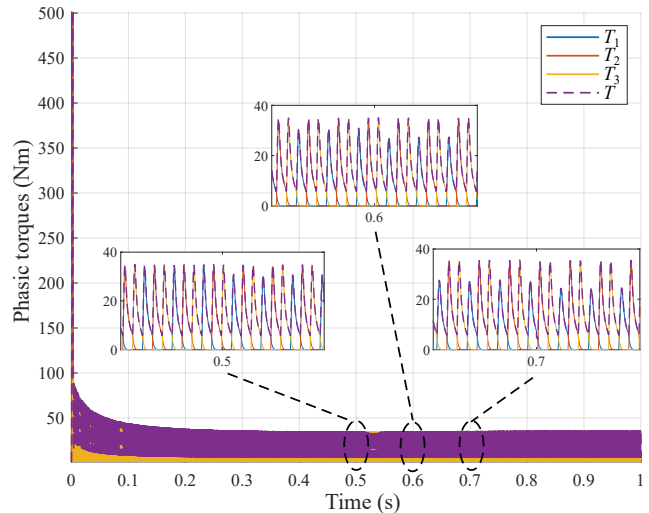


**Fig. 8:** Phasic torques in healthy and faulty cases.

## 6. Close Loop Fault Behavior

In this section, a backstepping type control is implemented using a speed regulator and three similar current regulators in continuous time. The adjustment parameters are numerous, it was therefore necessary to develop a strategy for choosing the adjustment parameters. This adjustment strategy depends on the context of operation and the use of our motor and can be represented in three minimisation steps: i) of the steady state errors of current regulators, ii) of the steady state error of the speed regulator and iii) of the torque ripple. The torque ripple also depends on the load torque,

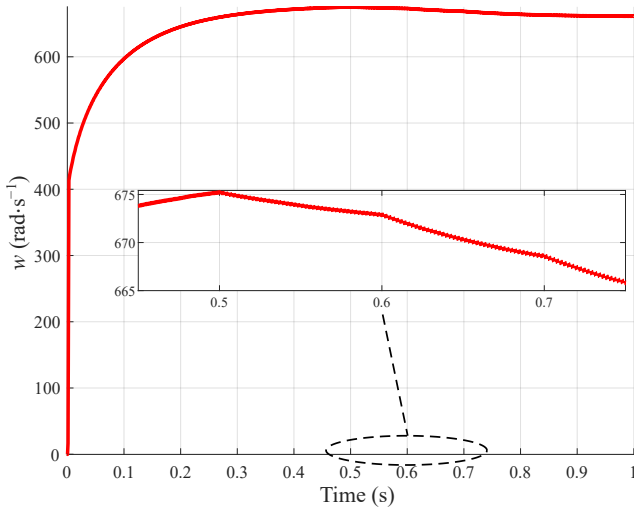


Fig. 9: Mechanical speed in healthy and faulty cases.

which is why a load torque has been set to obtain optimum ripple. Table 3 summarizes different adjustment parameters of the backstepping regulators.

Tab. 3: Adjustment parameters.

$C_w = 5 \cdot 10^3$
$C_i = 10^7$
$\theta_{on} = 45^\circ$
$\theta_{off} = 76.5^\circ$
$\theta_{ov} = 6^\circ$
$w^* = 300 \text{ rad}\cdot\text{s}^{-1}$
$T_L = 10 \text{ Nm}$

Figure 10 shows that the angular speed regulation error is very low and does not exceed 0.06 %, a zoom of this error shows that the damaged phase is responsible for the loss of speed of the 6/4 SRM but it still participates with the other two healthy phases to the regulation of angular speed.

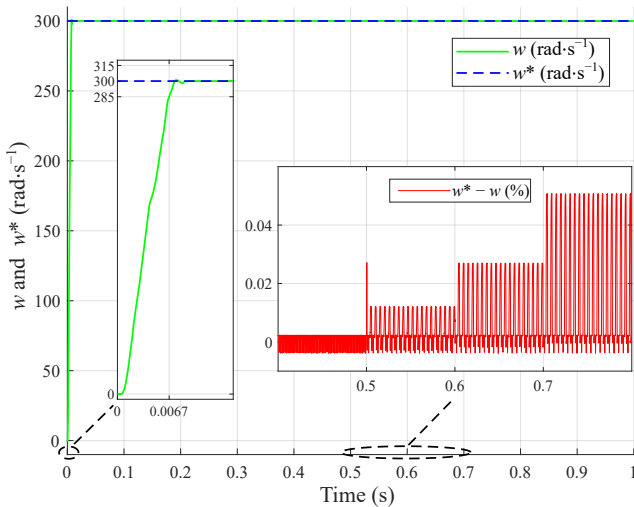


Fig. 10: Angular speeds in healthy and faulty cases.

Figure 11 shows that the dragging error during the backstepping control of the defective phase current regulator remains very low. The simulation shows a very interesting behavior of the currents of the non-defective phases 2 and 3.

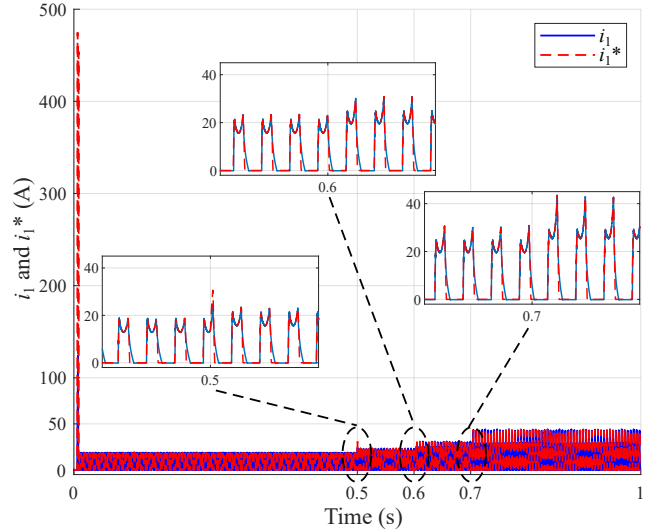


Fig. 11: Defective phase current in healthy and faulty cases.

Figure 12 shows that the three current setpoints are influenced by the fault in phase 1. The setpoint and phasic currents of phase 2 are much more influenced than those of phase 3. The three phases of the 6/4 SRM controlled with a backstepping regulator help each other to compensate for short-circuit faults. This behavior is due to the TSF strategy especially in the overlap angles, the setpoint torque of one phase influences the setpoint torque of the neighboring phase. The currents follow the same law of the torque through the TIM.

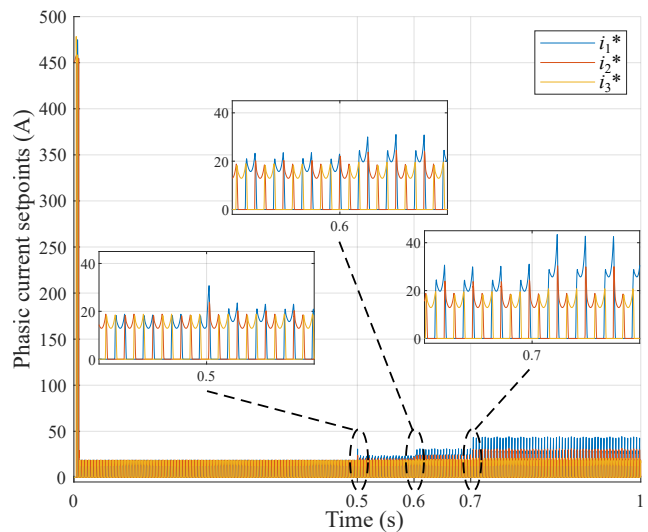


Fig. 12: Setpoint currents in healthy and faulty cases.

Table 4 summarizes the results of this simulation. In closed loop, a maximum short-circuit rate of 30 %

is used just to present the possibilities offered by this type of regulator. A study of extreme cases of short-circuit faults is not essential in this article because our objective is to allow a diagnosis of this type of fault before it becomes intolerable for this regulator-machine combination.

**Tab. 4:** RMS of phasic currents ( $T_L = 10$  Nm).

Cases	$i_1$	$i_2$	$i_3$
Healthy	9.2988	9.2520	9.2549
5 % of faulty	11.1585	9.4690	9.2551
10 % of faulty	13.6549	9.8560	9.2576
15 % of faulty	17.5790	10.3905	9.2551
20 % of faulty	24.3511	11.4588	9.2545
25 % of faulty	35.6146	13.2088	9.2590
30 % of faulty	60.2006	15.6794	9.2573

To allow supervision of this behavior, we draw a graphical representation of the results of the simulation of inter-turn short-circuit faults in phase 1. Figure 13 represents the evolution of the RMS values of the three phasic currents as a function of the ITSC percentage. It is correct that these values of RMS will change with the load torque considered as an external disturbance, this is why we have studied the behavior of these values according to this parameter. This law of variation is bijective for the defective phase current, so we can deduce the short-circuit rate from the RMS value of the current in faulty phase.

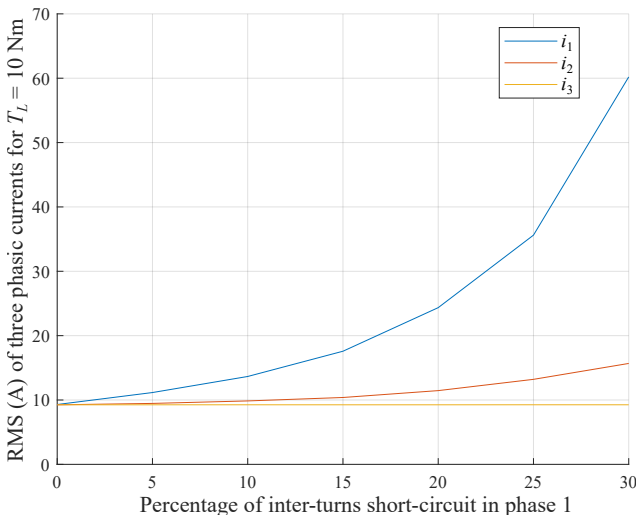


**Fig. 13:** Behavior of the RMS of phasic currents.

Figure 14 represents the evolution of the current of the defective phase with the percentage of short-circuit for different load torques. This law always remains bijective for the current of the defective phase when the load torque varies, so we can always deduce the short-circuit rate from the RMS value of the current.

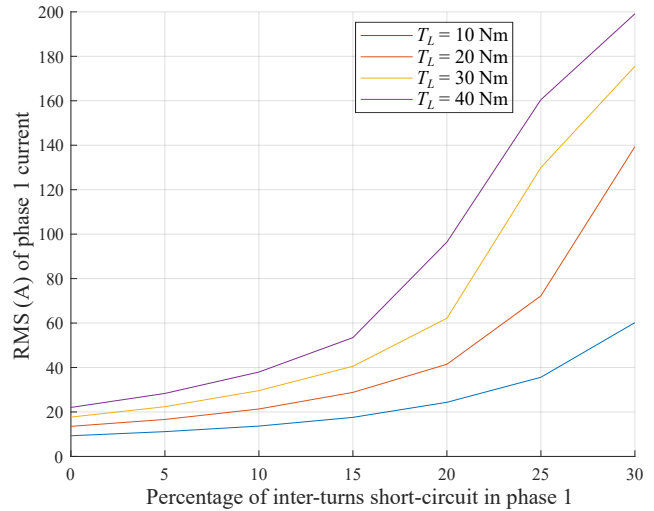


**Fig. 14:** Behavior of the RMS current values of phase 1.

## 7. Real Load Behavior and Practical Considerations

This section focuses on the behavior of the proposed machine controller in different scenarios. These include the presence of a load torque formed by a moment of inertia of  $2.92 \text{ kg}\cdot\text{m}^2$  [13] and a dry friction of 20 Nm disturbed by a sinusoidal ripple of 5 Nm of amplitude and  $30 \text{ rad}\cdot\text{s}^{-1}$  of pulsation corresponding to a linear speed of  $30 \text{ km}\cdot\text{h}^{-1}$  (about 20 mph) for wheels with a radius of 0.28 m [13]. The diagnosis of the ITSC fault must be done before introducing this real load at time 0.2 s. Our machine start with its own inertia, its own viscous friction and its own dry friction. The results of this simulations are given in Fig. 15, Fig. 16 and Fig. 17, which show an increase in the average amplitudes and ripples of phase currents, electromagnetic torque and mechanical speed error for this type of load, respectively.

The increase in mean values is due to the mechanical load and the increase in the amplitude of the ripples is due to the short circuit rate. The mechanical load introduces a speed ripple not exceeding 0.1 %. This value is very dominant on that introduced by the short-circuit fault which is less than 0.004 %. The article [14] presents a high frequency demodulation method for instantaneous angular speed estimation and gives quantization steps for different resolutions of optical encoders. A 4096 resolution encoder gives a quantization step equal to  $0.4 \mu\text{s}$  which is sufficient to follow the speed ripple due to the ITSC.

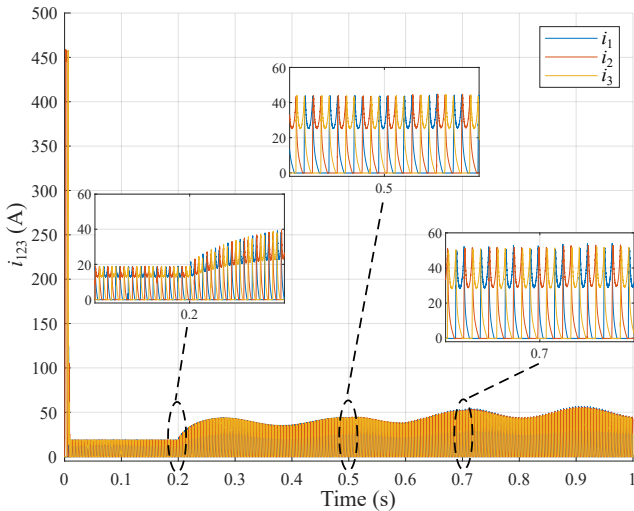


**Fig. 15:** Behavior of phase currents in the presence of a real load.

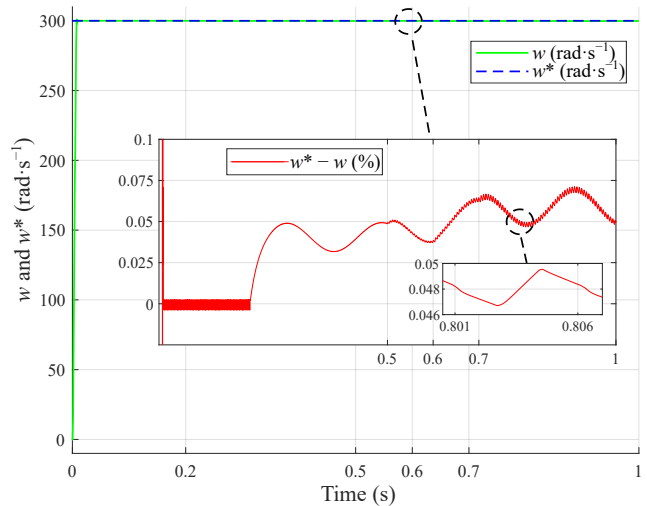


**Fig. 17:** Behavior of the speed error in the presence of real load.

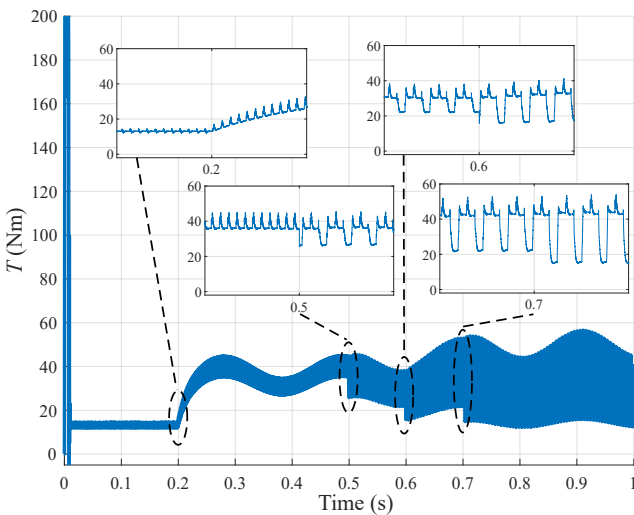


**Fig. 16:** Behavior of the electromagnetic torque in the presence of a real load.

## 8. Conclusion

The non-linear model of 6/4 SRM that we developed based on Legendre polynomials, was very useful for us to simulate the behavior of this type of switched reluctance motor in the presence of the inter-turn short-circuit fault. This model also allowed us to simulate backstepping-type speed regulation, which is very useful in electric cars on long-distance trips.

The simulation results show that the backstepping controller is very efficient for this type of non-linear systems with regard to stabilization, overshoot reduction, response time and precision, thus allowing satisfactory dynamic behavior. In addition, the controller parameters, when selected, provide good performance for a wide operating range, especially when faults appear.

This type of regulator is effective for fault tolerance, so it is very useful in electric cars to mask certain faults, especially in speed regulation on the motorway. This characteristic did not prevent us from proposing very useful indicators for the supervision of this type of regulator-machine association. Indeed, in these simplified concrete hypotheses, it turns out that it would be possible to use the RMS value of the phase currents as a fault indicator in the on-board computer of this type of car.

The results of the simulation with specific parameters were presented. Other possibilities of parameter values and parasitic phenomena related to the implementation should be considered in future work.

## Acknowledgment

The authors would like to thank the anonymous reviewers for their helpful and constructive comments that greatly contributed to improving the final version of the paper. They would also thank the Editors for their generous comments and support during the review process.

## Author Contributions

M.A. developed the theoretical formalism, performed the analytic calculations and performed the numerical simulations. Both M.A. and A.A. authors contributed to the final version of the manuscript. R.A. and J.B. supervised the project.

## References

- [1] GAN, C., J. WU, Y. HU, S. YANG, W. CAO and J. M. GUERRERO. New Integrated Multilevel Converter for Switched Reluctance Motor Drives in Plug-in Hybrid Electric Vehicles With Flexible Energy Conversion. *IEEE Transactions on Power Electronics*. 2017, vol. 32, iss. 5, pp. 3754–3766. ISSN 1941-0107. DOI: 10.1109/TPEL.2016.2583467.
- [2] CHICHATE, K. R., S. R. GORE and A. ZADEY. Modelling and Simulation of Switched Reluctance Motor for Speed Control Applications. In: *2020 2nd International Conference on Innovative Mechanisms for Industry Applications (ICIMIA)*. Bangalore: IEEE, 2020, pp. 637–640. ISBN 978-1-7281-4167-1. DOI: 10.1109/ICIMIA48430.2020.9074845.
- [3] TOUATI, Z., I. MAHMOUD and A. KHEDHER. Nonlinear Modelling of Switched Reluctance Machine. In: *2019 International Conference on Signal, Control and Communication (SCC)*. Hammamet: IEEE, 2019, pp. 256–261. ISBN 978-1-7281-3596-0. DOI: 10.1109/SCC47175.2019.9116143.
- [4] NIRGUDE, A., M. MURALI, N. CHAITHANYA, S. KULKARNI, V. B. Bhole and S. R. PATEL. Nonlinear mathematical modeling and simulation of Switched Reluctance Motor. In: *2016 IEEE International Conference on Power Electronics, Drives and Energy Systems (PEDES)*. Trivandrum: IEEE, 2017, pp. 1–6. ISBN 978-1-4673-8888-7. DOI: 10.1109/PEDES.2016.7914462.
- [5] NAITALI, A., A. AAMOUD and A. HAMMOUCH. Grey-box modelling and parameter estimation of switched reluctance motors. In: *2014 IEEE Conference on Control Applications (CCA)*. Juan Les Antibes: IEEE, 2014, pp. 352–357. ISBN 978-1-4799-7409-2. DOI: 10.1109/CCA.2014.6981371.
- [6] HUSAIN, I. and M. EHSANI. Torque ripple minimization in switched reluctance motor drives by PWM current control. *IEEE Transactions on Power Electronics*. 1996, vol. 11, iss. 1, pp. 83–88. ISSN 1941-0107. DOI: 10.1109/63.484420.
- [7] FERKOVA, Z., L. SUCHY and P. BOBER. Comparison of 6/4 and 12/8 switched reluctance motor models using direct torque control with torque lookup table. *Electrical Engineering*. 2020, vol. 102, iss. 1, pp. 75–83. ISSN 1432-0487. DOI: 10.1007/s00202-019-00775-z.
- [8] RUIWEI, Z., Z. YINGCHAO, Q. XISEN, L. TING and Z. ZHENGMING. Direct instantaneous torque control of switched reluctance motor based on adaptive backstepping. In: *2014 17th International Conference on Electrical Machines and Systems (ICEMS)*. Hangzhou: IEEE, 2014, pp. 567–572. ISBN 978-1-4799-5162-8. DOI: 10.1109/ICEMS.2014.7013535.
- [9] LIN, F.-J., S.-G. CHEN and C.-W. HSU. Intelligent Backstepping Control of Synchronous Reluctance Motor Drive System. In: *2018 International Automatic Control Conference (CACs)*. Taoyuan: IEEE, 2019, pp. 1–6. ISBN 978-1-5386-6278-6. DOI: 10.1109/CACS.2018.8606767.
- [10] RO, H.-S., K.-G. LEE, J.-S. LEE, H.-G. JEONG and K.-B. LEE. Torque Ripple Minimization Scheme Using Torque Sharing Function Based Fuzzy Logic Control for a Switched Reluctance Motor. *Journal of Electrical Engineering and Technology*. 2015, vol. 10, iss. 1, pp. 118–127. ISSN 2093-7423. DOI: 10.5370/JEET.2015.10.1.118.
- [11] BOUCHNAIF, J., K. GRARI, A. BENSLIMANE and F. JEFFALI. Analytical approach and thermal signature of Switched reluctance motor iron losses. *Materials Today: Proceedings*. 2020, vol. 27, iss. 4, pp. 3161–3166. ISSN 2214-7853. DOI: 10.1016/j.matpr.2020.04.031.
- [12] VINEETHA, P. L. S. and M. BALAJI. Fault Classification in SRM Drive Using Hilbert Transform. In: *International Conference on Power Engineering Computing and Control (PECCON)*. Chennai: Springer, 2021, pp. 121–133. ISBN 978-981-15-7241-8. DOI: 10.1007/978-981-15-7241-8\_10.
- [13] FAJRI, P., R. AHMADI and M. FERDOWSI. Equivalent vehicle rotational inertia used for electric vehicle test bench dynamic studies. In: *IECON 2012 - 38th Annual Conference on IEEE Industrial Electronics Society*. Montreal: IEEE, 2012, pp. 4115–4120. ISBN 978-1-4673-2421-2. DOI: 10.1109/IECON.2012.6389231.
- [14] BONNARDOT, F., K. LIZOUL, S. ERRAFIK, H. ANDRE and F. GUILLET. High frequency demodulation technique for instantaneous angular speed estimation. *Mechanical Systems and Signal Processing*. 2021, vol. 159, iss. 1, pp. 1–15. ISSN 1096-1216. DOI: 10.1016/j.ymssp.2021.107745.

## About Authors

**Mostafa ABDELOUHAB** (corresponding author) was born in Oujda, Morocco. He received his M.Sc.

from Mohammed fifth university, Rabat, Morocco in 2019. His research interests include machine control.

**Abdelilah ATTAR** was born in Oujda, Morocco. He received his engineer degree from National School of Applied Sciences in 2011. His research interests include machine control.

**Rachid ABOUTNI** was born in Guercif, Morocco. He received his Ph.D. from Mohammed first university, Oujda, Morocco in 2006. His research interests include machine control.

**Jamal BOUCHNAIF** was born in Oujda, Morocco. He received his Ph.D. from Mohammed first university, Oujda, Morocco in 2006. His research interests include machine control.